



1 **Source attribution of Arctic aerosols and associated Arctic**
2 **warming trend during 1980–2018**

3

4

5

6 Lili Ren¹, Yang Yang^{1*}, Hailong Wang², Rudong Zhang², Pinya Wang¹, Hong Liao¹

7

8

9

10 ¹Jiangsu Key Laboratory of Atmospheric Environment Monitoring and Pollution
11 Control, Jiangsu Collaborative Innovation Center of Atmospheric Environment and
12 Equipment Technology, School of Environmental Science and Engineering, Nanjing
13 University of Information Science and Technology, Nanjing, Jiangsu, China

14 ²Atmospheric Sciences and Global Change Division, Pacific Northwest National
15 Laboratory, Richland, Washington, USA

16

17

18

19

20 *Correspondence to yang.yang@nuist.edu.cn



21 **Abstract**

22 Observations show that the concentrations of Arctic sulfate and black carbon (BC)
23 aerosols have declined since the early 1980s, which potentially contributed to the recent
24 rapid Arctic warming. In this study, a global aerosol-climate model equipped with an
25 Explicit Aerosol Source Tagging (CAM5-EAST) is applied to quantify the source
26 apportionment of aerosols in the Arctic from sixteen source regions and the role of
27 aerosol variations in the Arctic surface temperature change over the past four decades
28 (1980–2018). The CAM5-EAST simulated surface concentrations of sulfate and BC in
29 the Arctic had a decrease of 43% and 23%, respectively, in 2014–2018 relative to 1980–
30 1984, mainly due to the reduction of emissions from Europe, Russia and Arctic local
31 sources. Increases in emissions from South and East Asia led to positive trends of Arctic
32 sulfate and BC in the upper troposphere. Changes in radiative forcing of sulfate and BC
33 through aerosol-radiation interactions are found to exert a +0.145 K Arctic surface
34 warming during 2014–2018 with respect to 1980–1984, with the largest contribution
35 (61%) by sulfate decrease, especially originating from the mid-latitude regions. The
36 changes in atmospheric BC outside the Arctic produced an Arctic warming of +0.062
37 K, partially offset by –0.005 K of cooling due to atmospheric BC within the Arctic and
38 –0.041 K related to the weakened snow/ice albedo effect of BC. Through aerosol-cloud
39 interactions, the sulfate reduction gave an Arctic warming of +0.193 K between the first
40 and last five years of 1980–2018, the majority of which is due to the mid-latitude
41 emission change. Our results suggest that changes in aerosols over the mid-latitudes of
42 the Northern Hemisphere have a larger impact on Arctic temperature than other regions



43 associated with enhanced poleward heat transport from the aerosol-induced stronger
44 meridional temperature gradient. The combined aerosol effects of sulfate and BC
45 together produce an Arctic surface warming of +0.297 K during 1980–2018, explaining
46 approximately 20% of the observed Arctic warming during the same time period.
47



48 **1. Introduction**

49 The Arctic has warmed rapidly since the 1980s, with a 1.5 K increase in the surface
50 air temperature, which is about two to four times faster than the global average
51 (Trenberth et al., 2007; Serreze et al., 2009). The significant rise in air and ground
52 temperatures occurred in phase with dramatic melting of Arctic sea ice and snow,
53 potentially contributing to Arctic amplification (Pithan and Mauritsen, 2014; Zhang et
54 al., 2019). A number of studies have examined possible mechanisms that caused the
55 rapid Arctic warming (Graversen et al., 2008; Screen and Ian, 2010; Screen and
56 Simmonds, 2010; Alexeev et al., 2012; Zhang et al., 2018). Observations and modeling
57 studies suggest that, although anthropogenic long-lived greenhouse gases (GHGs)
58 dominate the radiative forcing of the climate system, variations in black carbon (BC)
59 aerosol and other short-lived air pollutants are a good explanation for the faster Arctic
60 warming (Law and Andreas, 2007; Quinn et al., 2008; Shindell et al., 2008). In
61 particular, Shindell and Faluvegi (2009) indicated that Arctic warming was influenced
62 by the changing aerosol concentrations in the Arctic over the last three decades based
63 on model sensitivity experiments. The aerosols that caused Arctic warming are not only
64 from local emissions. Previous studies have shown that changes in long-range transport
65 of sulfate and BC aerosols from mid-latitude regions have caused strong wintertime
66 warming in the Arctic (e.g., Breider et al., 2014; Fisher et al., 2011; Shindell et al.,
67 2008). In addition, the mid-latitude aerosols can influence Arctic climate through
68 changing poleward heat transport (Navarro et al., 2016).

69 Observed and modeled seasonal cycles of aerosol concentrations at the remote



70 Arctic surface show a maximum in winter, a phenomenon commonly known as Arctic
71 Haze, and a minimum in summer (Law and Andreas, 2007; Quinn et al., 2007; Eckhardt
72 et al., 2015; Garrett et al., 2010; Sharma et al., 2006). The winter maximum has been
73 attributed to the long-range transport of anthropogenic pollution from the mid-latitudes
74 of the Northern Hemisphere and weak removal in the Arctic (Stohl, 2006; Wang et al.,
75 2014). In contrast, summer aerosol concentrations in the Arctic atmosphere reach a
76 minimum value due to a reduced poleward aerosol transport from the mid-latitudes and
77 efficient wet scavenging processes during the transport (Bourgeois and Bey, 2011;
78 Browse et al., 2012; Garrett et al., 2011). Anthropogenic aerosol species (e.g., sulfate,
79 BC and organic matter) can affect Arctic climate by disturbing the energy balance of
80 the earth system (Yang et al., 2019a). Sulfate aerosols directly scatter solar radiation
81 and indirectly influence cloud processes by serving as cloud condensation nuclei (Yang
82 et al., 2017a; Zamora et al., 2017; Zhao and Garrett, 2015). BC absorbs solar radiation
83 and warms the atmosphere (Bond et al., 2013; Yang et al., 2017b; Lou et al., 2019a),
84 which can increase or decrease cloud cover depending on the vertical distribution of
85 BC relative to clouds (e.g., McFarquhar and Wang, 2006; Lou et al., 2019b). When it
86 deposits on snow and ice, BC can reduce surface albedo and accelerate snow melt
87 (Flanner et al., 2007; Qian et al., 2015). Breider et al. (2017) estimated the aerosol
88 radiative forcing due to aerosol-radiation interactions in the Arctic and found that,
89 averaged over 2005–2010, the top-of-the-atmosphere (TOA) forcing is $-0.60 \pm$
90 0.02 Wm^{-2} for sulfate and $+0.44 \pm 0.04 \text{ Wm}^{-2}$ for BC over the Arctic.

91 Analysis of long-term changes in sulfate and BC can help to gain a comprehensive



92 understanding of their past and present impacts on the Arctic climate. In situ
93 observations of sulfate and BC concentrations in the Arctic (e.g., at Alert, Barrow,
94 Station Nord, and Zeppelin) have shown a declining trend since the 1980s (Gong et al.,
95 2010; Heidam et al., 1999; Hirdman et al., 2010; Quinn et al., 2009; Sharma et al., 2004;
96 Sharma et al., 2006; Sinha et al., 2017; Sirois and Barrie, 1999). Based on the chemical
97 transport model GEOS-Chem simulations, Breider et al. (2017) found that annual
98 sulfate and BC concentrations decreased by 2–3% per year over the Arctic. McConnell
99 et al. (2007) presented a historical BC trend derived from ice-core records, showing
100 that BC concentration had been declining steadily after the peak around 1910.

101 Source attribution analysis of atmospheric aerosols in the Arctic, which can help
102 to understand aerosol trends, is extremely important for air pollution research. There is
103 less local anthropogenic aerosol emission in the Arctic region than in polluted regions
104 of the world. Pollutants in the Arctic are generally from mid-latitude areas by long-
105 distance transport (Fisher et al., 2011; Wang et al., 2014). Recent studies have found
106 that Arctic aerosols mainly originated from Eurasia, Southeast Asia, Siberia and North
107 America (Fisher et al., 2011; Qi et al., 2017; Sharma et al., 2013; Stohl, 2006). The
108 contribution of Eurasia to Arctic sulfate and BC aerosols concentration is dominant in
109 the lower atmosphere, while South and Central Asia contributed the most at high
110 altitudes (e.g., Wang et al., 2014). In general, Northern Europe and Russia, with large
111 industrial emissions, are the main source region of Arctic BC aerosols in spring (Rahn
112 et al., 1977; Rahn, 1981; Raatz and Shaw, 1984; Barrie, 1986; Koch and Hansen, 2005;
113 Sharma et al., 2006; Stohl, 2006). In the past few decades, anthropogenic emissions



114 have changed rapidly, with a decrease in Europe and North America and an increase in
115 South and East Asia. This may have had an important impact on the Arctic aerosols and
116 climate (Breider et al., 2014).

117 In this study, the global aerosol-climate model CAM5 (Community Atmosphere
118 Model, version 5) equipped with an Explicit Aerosol Source Tagging (CAM5-EAST)
119 is used to examine the attribution of Arctic aerosols to 16 different source regions and
120 the aerosol-related Arctic warming during 1980–2018. We focus on changes in sulfate
121 and BC near-surface concentrations, total column burden, and radiative forcing as well
122 as their impacts on the surface temperature over the Arctic. Modeled and observational
123 sulfate and BC concentrations at remote Arctic stations are compared. CAM5-EAST
124 tagging results are used to quantify the contributions of different sources to the decadal
125 changes in Arctic sulfate and BC surface concentrations and vertical profiles. Based on
126 the Arctic climate sensitivity factors, we estimate the responses of the Arctic surface
127 temperature to the variations in sulfate and BC during the analyzed time periods.

128 **2. Methodology**

129 **2.1 Model Description and Experimental Setup**

130 The global aerosol-climate model CAM5, which is the atmospheric component of
131 the earth system model CESM (Community Earth System Model) developed at the
132 National Center for Atmospheric Research (NCAR), is used to simulate Arctic aerosols
133 and climate for years 1980–2018 (after one-year model spin-up). In this model version,
134 mass concentrations of sulfate, BC, primary organic aerosol (POA), second organic
135 aerosol (SOA), mineral dust, and sea salt are predicted with a three-mode modal aerosol



136 module. Aerosol number concentration is also predicted for each mode. Particles in the
137 different size modes are assumed to be externally mixed and internally mixed in the
138 same mode. The optical properties and radiative impact of aerosols are calculated online.
139 The model also includes climate effects of aerosols through aerosol-radiation and
140 aerosol-cloud interactions. In this study, the model is configured to run at a horizontal
141 grid of 1.9° latitude \times 2.5° longitude with 30 vertical layers up to 3.6 hPa.

142 The CAM5 simulation is conducted with prescribed time-varying solar radiation, sea
143 surface temperature, sea ice concentration, GHGs, and emissions of aerosols and their
144 precursor gases. In order to better reproduce the aerosol transport driven by large-scale
145 circulations in the model, the wind field is nudged toward the MERRA-2 (Modern Era
146 Retrospective-Analysis for Research and Applications, Version 2) reanalysis
147 (Rienecker et al., 2011; Gelaro et al., 2017) at a 6-hourly relaxation timescale. Radiative
148 forcing due to aerosol-radiation interactions is calculated as the difference of clear-sky
149 net radiative fluxes at TOA between two separate diagnostic calculations, including and
150 excluding a specific aerosol in the radiative transfer calculation, respectively (Ghan et
151 al., 2012).

152 **2.2 Explicit Aerosol Source Tagging and Source Regions**

153 The Explicit Aerosol Source Tagging (EAST) was implemented in CAM5 to quantify
154 the source-receptor relationships of aerosols in recent studies (Wang et al., 2014; Yang
155 et al., 2017a,b; 2018a,b,c). All physical, chemical and dynamical processes of aerosols
156 for each tagged source region or sector are considered independently and consistently
157 by using additional sets of aerosol variables in CAM5-EAST, which is different from



158 the widely used emission sensitivity method that assumes a linear response to emission
159 perturbation or the indirect method of tracing long-lived constituents associated with
160 particular sources. Without such assumption of linear response or constant decaying
161 rate, EAST is more physically accurate than the source attribution methods mentioned
162 above. In this study, sulfate and BC are explicitly tracked throughout the processes from
163 source emissions to deposition in a single model simulation.

164 We focus on the Arctic (66.5°N – 90°N) as the receptor region in this study. According
165 to source region definition of the Hemispheric Transport of Air Pollution model
166 experiment phase 2 (HTAP2), sulfate and BC from 16 regions are tagged (Fig. 1):
167 Europe (EUR), North America (NAM), Central America (CAM), South America
168 (SAM), North Africa (NAF), South Africa (SAF), the Middle East (MDE), Southeast
169 Asia (SEA), Central Asia (CAS), South Asia (SAS), East Asia (EAS), Russia-Belarus-
170 Ukraine (RBU, hereafter Russia), Pacific-Australia-New Zealand (PAN), the Arctic
171 (ARC), Antarctic (ANT), and Non-Arctic/Antarctic Ocean (OCN). Note that the OCN
172 tag includes sources from oceans and volcanic eruptions.

173 **2.3 Aerosol and Precursor Emissions**

174 In order to simulate the long-term temporal variations in aerosols, historical
175 anthropogenic (Hoesly et al., 2018) and biomass combustion (van Marle et al., 2017)
176 emissions of aerosols and precursor gases during 1980–2014 are used in the simulation
177 following the CMIP6 (Coupled Model Intercomparison Project Phase 6) protocol. For
178 the most recent years (2015–2018), yearly interpolated emissions from the SSP2-4.5
179 scenario, which is the modest scenario compared to other SSPs and is widely utilized



180 in many MIPs (O'Neill et al., 2016) are used. Figures 1 and 2 show the spatial
181 distribution and time series of annual anthropogenic SO₂ and BC emissions,
182 respectively, during 1980–2018, from the 16 source regions. The global total
183 anthropogenic SO₂ and BC emission rates, averaged over 1980–2018, are 118.4 Tg yr⁻¹
184 and 8.1 Tg yr⁻¹, respectively. SO₂ emissions are relatively high in East Asia (23.6 Tg
185 yr⁻¹), Europe (15.8 Tg yr⁻¹) and North America (15.4 Tg yr⁻¹), while BC emissions show
186 a high mean value in East Asia (1.8 Tg yr⁻¹), South Africa (1.6 Tg yr⁻¹) and South Asia
187 (0.9 Tg yr⁻¹). Comparing 2014–2018 to 1980–1984, global anthropogenic SO₂ emission
188 was reduced by 32.2 Tg yr⁻¹ (24.8% relative to 1980–1984). The largest decreases took
189 place in Europe (83.0%), North America (80.7%) and Russia (74.8%). In East Asia,
190 emissions of anthropogenic SO₂ were increased by a factor of 2.7 from 1980 to 2014,
191 followed by a decreasing trend after 2014 due to stricter air pollution regulations. The
192 global anthropogenic BC emission increased from 6.5 Tg yr⁻¹ in 1980 to a peak of 9.6
193 Tg yr⁻¹ in 2014, followed by a slow decline, with an overall increase of 42% between
194 the first and last five years of 1980–2018. Regionally, compared to 1980–1984,
195 averaged BC emissions in 2014–2018 in Europe, Russia and the Arctic decreased by
196 45.2%, 44.1% and 38.3%, respectively, while BC emissions in East Asia and South Asia
197 almost increased by a factor of 2. Within the Arctic, SO₂ and BC emissions decreased
198 by 5.8% and 38.3%, respectively.

199 **2.4 Model Evaluation**

200 To assess the ability of the model to simulate Arctic sulfate and BC, Figs. 3 and 4
201 compare simulated near-surface concentrations of sulfate and BC, respectively, in



202 spring and summer during 1980–2018 with observations at five Arctic stations: Alert
203 (82°N, 62°W), Station Nord (81°N,16°W), Barrow (71°N,156°W), Ny-Alesund
204 (78°N,11°E) and Kevo (69°N,27°E). The observations are derived from European
205 Monitoring and Evaluation Programme and World Data Centre for Aerosols database
206 (<http://ebas.nilu.no>) and Breider et al. (2017).

207 Overall, the sulfate and BC concentrations in spring is higher than those in summer,
208 mainly due to lower removal rate and more efficient transport (Stohl, 2006). The model
209 underestimates aerosol concentrations in spring, likely due to biases in simulated
210 precipitation and aerosol wet removal during the transport to high latitudes. All sites
211 show that sulfate concentrations decrease during the analyzed time period and BC
212 decreases at specific sites, which can be explained by the reduction of non-local
213 emissions as illustrated by the source attribution. Compared to the observed values, the
214 model can reasonably simulate the time variations of sulfate and BC in the Arctic but
215 the magnitude at some of the sites is largely underestimated. The Kevo site, which is
216 close to Western Eurasia, is the only site that has both sulfate and BC data for more than
217 30 years. At this site, the simulated sulfate and BC in spring (summer) decreased at a
218 rate of -3.18% (-1.92%) and -2.89% (-1.74%) per year, which is similar to -4.37% (-
219 3.26%) and -3.01% (-2.82%) per year from observations. The Alert site has 33-year
220 sulfate observations, where the simulated sulfate concentrations declined at a rate of -
221 2.08% (-2.00%) per year, consistent with the observed decreasing trends of -2.89% (-
222 0.47%) per year.

223 Observational data are very limited in the Arctic, especially the long-term



224 observations. The available BC measurements are equivalent elemental carbon (EBC),
225 which is usually obtained by converting the light absorbed by the particles accumulated
226 on the ground instrument filter into the BC concentration. The uncertainty in optical
227 properties of BC makes this conversion challenging. Other light absorbing substances,
228 such as dust and organic carbon, also affect the BC measurements, so EBC would tend
229 to be higher than the actual BC concentration. Researchers found that BC observations
230 could be biased by 30% to 200% (Sharma et al., 2017; Sinha et al., 2017) due to the
231 inclusion of other light absorption components in the atmosphere. Shindell et al. (2008)
232 and Koch et al. (2009) found great differences between the current models and
233 observations of Arctic BC and sulfate through multi-model comparison studies,
234 including incorrect seasonality and order of magnitude biases. Given the large apparent
235 discrepancies in BC for all models, it is difficult to determine the relative authenticity
236 of the models using currently available data (Shindell et al., 2008).

237 **3. Source Apportionment of Aerosols in the Arctic**

238 The near-surface concentrations of sulfate and BC over the Arctic can be
239 quantitatively attributed to both Arctic local emissions and remote sources outside the
240 Arctic through the source tagging in CAM5-EAST. The absolute and relative source
241 contributions are shown in Fig. 5. Arctic local emissions and sources near the Arctic
242 (e.g., Europe and Russia) are the main contributors to the near-surface concentrations
243 of Arctic sulfate and BC. Relative to 1980–1984, the simulated annual sulfate
244 concentration over the Arctic has a decrease of 42.8% in 2014–2018 (Table 1). Sulfate
245 concentration shows a considerable decreasing trend from 1980 to 2000 and then slows



246 down after 2000. The decrease in sulfate during this time period primarily results from
247 the reduction in emissions from Europe and Russia, which contributes to -18.6% and -
248 18.8% of the decline of the Arctic sulfate concentrations, respectively. The change in
249 emissions from Central Asia and North America, respectively, explains -1.6% and -3.4%
250 of the reduced concentration.

251 Simulated Arctic BC concentration also shows a considerable decline before 2000,
252 but a slight rise after 2000. Overall, the average concentration of BC in the Arctic had
253 a decrease of 22.98% in 2014–2018 relative to 1980–1984, mainly due to the reductions
254 in emissions originating from the Arctic and Russia, which lead to 9.32% and 14.91%
255 of the concentration decrease (Table 1). Sources in Europe, North America, and East
256 Asia account for the changes in Arctic near-surface BC concentration in range of ± 1 –
257 3%. The remaining source regions have no substantial impact on the BC concentration
258 in the Arctic (total contribution less than 2%) due to weak emission strength or long
259 transport pathways. Since the Arctic sulfate and BC aerosol concentrations contributed
260 by non-local sources have been reducing, the fractional contribution of Arctic local
261 source increased from 33.6% and 53.4% to 55.1% and 57.3%, respectively. To further
262 reduce present-day or future aerosols in the Arctic, efforts can be made to control the
263 local sources in the Arctic.

264 Aerosols are often transported across continents in the free troposphere rather than
265 near the surface, resulting in a higher relative contribution of non-local sources to the
266 aerosol concentration at higher altitudes than near the surface. Figure 6 shows the
267 vertical profiles of absolute and relative contributions of major source regions to sulfate



268 and BC concentrations in the Arctic. Different source regions have very distinct vertical
269 distributions of their contributions. The largest contribution of East and South Asia
270 emissions is at 8-10 km, accounting for about two thirds of the Arctic aerosol
271 concentrations at this height, which is consistent with results from other models (e.g.,
272 Shindell et al., 2008). Emissions from the Arctic and Russia account for the majority of
273 Arctic sulfate and BC concentrations below 2 km and 6 km, respectively. The
274 contributions of emissions from Europe and North America are mainly located below
275 10 km. As the source emissions vary with time, the vertical aerosol concentrations
276 contributed by individual sources also change.

277 The changes in source contributions to the annual mean vertical profile of sulfate and
278 BC concentrations over the Arctic between 2014–2018 and 1980–1984 are shown in
279 Fig. 7. Due to the effective emission reduction, the contribution from Europe and Russia
280 to the Arctic sulfate below 6 km was each decreased by nearly $0.1 \mu\text{g m}^{-3}$ in 2014–2018,
281 compared to 1980–1984. North America contribution also had a slight decline below 2
282 km. Contributions from South and East Asia increased at the upper troposphere between
283 10–15 km, which is consistent with the increase in emissions over these regions, leading
284 to a combined increase in sulfate concentration of up to $0.1 \mu\text{g m}^{-3}$ at the upper levels
285 of the Arctic. The BC concentration below 2 km contributed by Arctic and Russia
286 emissions each had a decrease of up to 2 ng m^{-3} , which dominated the decrease of BC
287 concentration in the Arctic lower atmosphere. As with sulfate, BC concentrations
288 contributed by East Asia and South Asia show an increasing trend in the high altitudes,
289 mainly due to increased emissions in these two regions, offsetting the decrease in



290 column burden owing to the reduced concentration in the lower altitudes.

291 Linear trends of the annual near-surface concentrations and column burden of sulfate
292 and BC from 1980 to 2018 are shown in Fig. 8 and the individual source contributions
293 to these trends are summarized in Table 2. During 1980–2018, simulated Arctic near-
294 surface concentration and column burden of sulfate decreased by 20% and 13 % per
295 decade, respectively. Due to the air pollution regulations in Europe and dissolution of
296 the former Soviet Union, reductions in emissions from Europe and Russia led to
297 decreasing trends of 7–10% per decade in the near-surface concentration and column
298 burden of sulfate, having the largest contributions to sulfate trends among all tagged
299 source regions. In addition, the change in North America emissions contributed to a 2–
300 4% per decade decreasing trend in the Arctic sulfate concentration and burden, which
301 is related to its emission control since 1980s. South and East Asia together contributed
302 to an increase of total Arctic sulfate burden at a rate of 8% per decade, associated with
303 the emission rise during this time period. The near-surface concentration of Arctic BC
304 has a decreasing trend of 12% per decade during 1980–2018, mostly driven by the
305 decreases in contributions from Russia and Arctic local emissions (6% per decade each).
306 For BC column burden, the decreasing trends contributed by the reductions in emissions
307 from Russia and Europe are offset by the increasing trends caused by emission increases
308 in East and South Asia, resulting in an insignificant change of total BC burden during
309 1980–2018.

310 **4. Aerosol radiative forcing and associated Arctic warming**

311 Both sulfate and BC influence the Arctic climate through perturbing atmospheric and



312 surface radiation balance. The spatial distribution of the climatological mean TOA
313 radiative forcing due to aerosol-radiation interactions (RF_{ari}) of sulfate and BC during
314 1980–2018 is shown in Fig. 9. The Arctic sulfate exerts a negative RF_{ari} primarily by
315 scattering incoming solar radiation back into the space, with the forcing in range of -
316 $0.4\sim 0\text{ Wm}^{-2}$, while BC can absorb solar radiation in the atmosphere and leads to a
317 positive RF_{ari} of $0.1\sim 0.4\text{ Wm}^{-2}$ in the Arctic. In the high and mid-latitudes of the
318 Northern Hemisphere, the RF_{ari} of sulfate over Europe and Russia is in the range of -
319 $1.0\sim 0.4\text{ Wm}^{-2}$. Sulfate RF_{ari} over North America varies from -0.2 Wm^{-2} to -1.0 Wm^{-2} .
320 The negative RF_{ari} of sulfate over East Asia is more than -1.0 Wm^{-2} , mainly due to the
321 high sulfate concentrations. BC over Europe, Russia and Central Asia exerts a positive
322 RF_{ari} of $0.4\sim 1\text{ Wm}^{-2}$. The BC RF_{ari} over East Asia reaches a high value over 1.0 Wm^{-2} .

323 Previous studies have suggested that Arctic climate responds not only to Arctic local
324 forcings but also to forcings outside the Arctic due to the meridional energy transport
325 change (Navarro et al., 2016). To estimate the relative roles of recent aerosol trends in
326 the Arctic warming, we look into the temporal variation of annual mean RF_{ari} of sulfate
327 and BC in different latitude bands during 1980–2018 (Fig. 10). Within the Arctic
328 ($66.5^{\circ}\text{N}\sim 90^{\circ}\text{N}$), the negative RF_{ari} of sulfate decreases from -0.21 Wm^{-2} in 1980–1984
329 to a moderate value of -0.10 Wm^{-2} in 2014–2018, indicating a warming effect in the
330 Arctic from the local sulfate change. Over the mid-latitudes ($28^{\circ}\text{N}\sim 66.5^{\circ}\text{N}$), the sulfate
331 RF_{ari} decreases from -0.87 Wm^{-2} to -0.53 Wm^{-2} between the first and last five years of
332 1980–2018, while the magnitude of the sulfate RF_{ari} in the tropical region ($28^{\circ}\text{S}\sim 28^{\circ}\text{N}$)
333 increases from -0.52 Wm^{-2} to -0.60 Wm^{-2} . The positive BC RF_{ari} increases from 0.55



334 Wm^{-2} to 0.74 Wm^{-2} in the mid-latitudes and from 0.51 Wm^{-2} to 0.76 Wm^{-2} in the tropics,
335 while the BC RF_{ari} over the Arctic has no obvious change during this time period.

336 Systematic assessment of the impact of aerosols on Arctic warming since 1980s
337 requires quantifying the Arctic temperature responses to changes in radiative forcing of
338 different aerosol species over different regions. Here, we apply Arctic climate
339 sensitivity factors, defined as the Arctic temperature response per unit radiation, for
340 each short-lived climate forcers over the Arctic, mid-latitudes of the Northern
341 Hemisphere, tropics and Southern Hemisphere from Sand et al. (2016) and Shindell
342 and Faluvegi (2009) to calculate the recent Arctic surface temperature change related
343 to the variations in sulfate and BC radiative forcings over the different latitude bands
344 during 1980–2018 (Fig. 11 and Table 3). This method has been widely adopted to
345 examine the Arctic temperature response to aerosol forcings (e.g., Breider et al., 2017;
346 Flanner, 2013; Sand et al., 2016; Shindell and Faluvegi, 2009; Yang et al., 2018c).

347 It is estimated that, between 1980–1984 and 2014–2018, changes in total RF_{ari} of
348 sulfate and BC produce a surface warming of $+0.145 \text{ K}$ over the Arctic, with $+0.088 \text{ K}$
349 (61%) contributed by the sulfate forcing change and the remaining explained by the BC
350 forcing change. The sulfate-related Arctic warming is mainly due to the decrease in
351 sulfate in mid-latitudes that enhances the temperature gradient between the mid-
352 latitudes and Arctic, resulting in a strengthened meridional heat transport and, therefore,
353 the Arctic warming of $+0.059 \text{ K}$. The change in Arctic local RF_{ari} of sulfate provides
354 $+0.035 \text{ K}$ of the surface warming, while the forcing change in the tropics has a
355 negligible influence on the Arctic temperature change. The Arctic temperature



356 responses to increases in BC RF_{ari} over the mid-latitudes and tropics are +0.029 K and
357 +0.031 K, respectively, related to the enhanced poleward heat transport from the
358 warming radiative impact in the mid-latitudes, while changes in the Arctic BC RF_{ari}
359 only exert a weak cooling of -0.005 K. Overall, the RF_{ari} change over the mid-latitudes
360 provides the strongest warming effect (+0.088K) to the Arctic compared to other
361 latitude bands, owing to the aerosol-induced increase in the poleward heat transport.

362 While the results above focus on the effects of aerosol-radiation interactions, the
363 aerosol-cloud interactions (RF_{aci}) and BC snow/ice albedo effects can also influence
364 Arctic climate. Sulfate RF_{aci} is estimated by scaling sulfate RF_{ari} based on the ratio of
365 sulfate RF_{aci} and RF_{ari} over different latitudes from Sand et al. (2016). Within the Arctic,
366 the magnitude of negative TOA RF_{aci} of sulfate decreases from -0.48 Wm^{-2} in 1980–
367 1984 to -0.23 Wm^{-2} in 2014–2018, indicating a warming effect due to the local sulfate
368 change. Over the mid-latitudes, the sulfate RF_{aci} decreases from -2.46 Wm^{-2} to -1.49
369 Wm^{-2} between the first and last five years of 1980–2018, while the magnitude of the
370 sulfate RF_{aci} in the tropical region increases from -1.78 Wm^{-2} to -2.08 Wm^{-2} . The
371 positive RF due to BC in snow/ice decreases from 0.34 Wm^{-2} in 1980–1984 to 0.29
372 Wm^{-2} in 2014–2018 over the Arctic, while that over the mid-latitudes increases from
373 0.19 Wm^{-2} to 0.23 Wm^{-2} .

374 Based on the Arctic climate sensitivities, impacts of changes in radiative forcing due
375 to aerosol-cloud interactions of sulfate are also estimated. The sulfate RF_{aci} provides an
376 Arctic warming of +0.193 K between 1980–1984 and 2014–2018, with +0.165 K
377 contributed by the RF_{aci} change over the mid-latitudes and +0.078 K resulting from the



378 Arctic RF_{aci} change. It should be noted that aerosol-cloud interactions at high latitude
379 regions are complicated and highly uncertain in climate models. The temperature
380 changes presented here only provide a very rough estimate. BC in snow/ice reduces
381 surface albedo and increases snow/ice melt (Flanner et al., 2007; Qian et al., 2015). Due
382 to the decrease in Arctic BC concentration and deposition, BC concentration in the
383 Arctic snow has been decreasing (e.g., Zhang et al., 2019). The weakened BC snow/ice
384 albedo effect leads to an Arctic cooling of -0.061 K, while the mid-latitude BC in
385 snow/ice causes an Arctic warming of $+0.019$ K. The total BC snow/ice albedo effects
386 result in an Arctic surface temperature change of -0.041 K during 1980–2018, partially
387 offsetting the solar absorbing effect of BC in the atmosphere. Combining all the effects,
388 we estimate that between 1980 and 2018, sulfate and BC contribute a total of $+0.297$ K
389 to the Arctic surface temperature change, approximately 20% of the observed Arctic
390 warming during this period.

391 **5. Conclusions and discussion**

392 The Arctic has warmed rapidly since the 1980s, with the surface air temperature
393 increasing by 1.5 K. Many studies have examined possible mechanisms that caused the
394 Arctic warming, but many are still on debate. In this study, we use a global aerosol-
395 climate model equipped with the Explicit Aerosol Source Tagging module (CAM5-
396 EAST) to quantify the source attribution of aerosols in the Arctic and the aerosol-related
397 Arctic warming during 1980–2018. The model can reasonably simulate the spatial
398 distribution and temporal variation of the Arctic near-surface sulfate and BC
399 concentrations compared with several site measurements, while it underestimates the



400 magnitude of sulfate and BC to some extent.

401 Compared to 1980–1984, the simulated annual average of sulfate and BC
402 concentrations over the Arctic in 2014–2018 had a decrease of 42.8% and 23.0%,
403 respectively. The decrease in emissions from Europe and Russia contributed -18.6%
404 and -18.8% of the near-surface sulfate concentration decrease (out of -42.8%) and the
405 reduction in Arctic local emissions and emission from Russia led to -9.3% and -14.9%
406 of the BC concentration reduction (out of -23.0%), respectively. In 2014–2018,
407 increases in emissions from South and East Asia together contributed to an increase of
408 sulfate and BC concentrations up to $0.1 \mu\text{g m}^{-3}$ and 2 ng m^{-3} , respectively, at the upper
409 troposphere, compared to 1980–1984. The contribution of Europe and Russia emissions
410 to the Arctic sulfate concentration each had a decrease of about $0.1 \mu\text{g m}^{-3}$ under 6 km.
411 Below 2 km, the BC concentration contributed by emissions from Arctic and Russia
412 each had a decrease of up to 2 ng m^{-3} . Simulated sulfate near-surface concentration and
413 column burden had a decreasing trend of 20% per decade and 13% per decade,
414 respectively, in the Arctic during 1980–2018, mainly driven by the reductions in
415 emissions from Europe and Russia, both of which led to decreasing trends at a rate of
416 7–10% per decade. Due to the decreases in contributions from Russia and Arctic local
417 emissions (6% per decade each), the near-surface concentration of Arctic BC presents
418 a decreasing trend of 12% per decade during 1980–2018.

419 Aerosols within and outside the Arctic can influence the Arctic climate through
420 changing the radiative balance. The magnitude of negative TOA RF_{ari} of sulfate over
421 the Arctic decreased from -0.21 Wm^{-2} in 1980–1984 to -0.10 Wm^{-2} in 2014–2018. Over



422 the mid-latitudes, the sulfate RF_{ari} magnitude decreased from -0.87 Wm^{-2} to -0.53 Wm^{-2} ,
423 2 , while the sulfate RF_{ari} over the tropics increased from -0.52 Wm^{-2} to -0.60 Wm^{-2} . The
424 positive BC RF_{ari} in the mid-latitudes and tropics increased from 0.55 Wm^{-2} and 0.51
425 Wm^{-2} to 0.74 Wm^{-2} and 0.76 Wm^{-2} , respectively, while that over the Arctic had no
426 significant change during this time period.

427 By applying Arctic climate sensitivity factors obtained from the literature to the
428 variations in aerosol radiative forcing, the aerosol-induced Arctic surface temperature
429 change is estimated in this study. During 1980–2018, through aerosol-radiation
430 interactions, sulfate and BC together produced a $+0.145 \text{ K}$ warming to the Arctic,
431 $+0.088 \text{ K}$ (61%) of which is contributed by sulfate. The decrease in sulfate in mid-
432 latitudes led to an increase in Arctic temperature of $+0.059 \text{ K}$, whereas the Arctic local
433 sulfate provided $+0.035 \text{ K}$ of the surface warming. The Arctic temperature responses to
434 changes in atmospheric BC over the mid-latitudes and tropics are $+0.029 \text{ K}$ and $+0.031$
435 K , respectively, while changes BC in the Arctic atmosphere only exert a weak cooling
436 of -0.005 K . Through aerosol-cloud interactions, sulfate exerted an Arctic warming of
437 $+0.193 \text{ K}$ during 1980–2018, with $+0.165 \text{ K}$ contributed by the forcing change over the
438 mid-latitudes and $+0.078 \text{ K}$ due to the forcing change over the Arctic. Therefore,
439 changes in aerosols over the mid-latitudes had the largest impact on the Arctic
440 temperature than other regions during 1980–2018 through enhancing meridional
441 temperature gradient and therefore poleward heat transport, followed by changes in
442 Arctic local aerosol forcings. Due to the decrease in Arctic BC concentration, the
443 weakened BC snow/ice albedo effect led to an Arctic cooling of -0.061 K , partially



444 offset by Arctic warming of +0.019 K induced by the BC snow/ice albedo effect over
445 the mid-latitudes. Combining all aerosol effects, sulfate and BC together produced a
446 total of +0.297 K in the Arctic surface temperature change during 1980–2018,
447 explaining approximately 20% of the observed Arctic warming during this period.

448 There are a few sources of uncertainty in the results presented in this study. As
449 discussed above, the model underestimates the near-surface sulfate and BC
450 concentrations over the Arctic, probably due to an overly aerosol wet removal during
451 the long-range transport (e.g., Wang et al., 2013), uncertainties in aerosol emissions,
452 and biases in observations. Here we only discussed the effects of sulfate and BC on the
453 Arctic surface temperature without considering other aerosol species, due to large
454 uncertainties in the simulation of second organic aerosols and the lack of other aerosol
455 treatments (e.g., nitrate) in current model version. These may lead to biases of the
456 aerosol climate effects in this study. In addition, we estimated the temperature response
457 of the Arctic to the aerosol-induced TOA radiative forcing change based on the climate
458 sensitivity factors derived from the literature. For more accurate estimation of the
459 aerosol-related Arctic warming, the coupled model configuration with free running
460 simulations should be conducted in the future. The RF_{ari} calculation follows Ghan et al.
461 (2012), which falls into the definition of effective RF_{ari} (ERF_{ari}), while the climate
462 sensitivity factors were calculated based on the stratospherically adjusted radiative
463 forcing. Considering that the assessment for adjusted RF_{ari} ($-0.35 \pm 0.5 \text{ W m}^{-2}$) is
464 slightly lower than that for ERF_{ari} ($-0.45 \pm 0.5 \text{ W m}^{-2}$) (Boucher et al., 2013), the
465 temperature response could be relatively smaller than estimated here. The relatively



466 low model resolution may not capture the complexity of the Arctic terrain (Yang et al.,
467 2018c), which also induces uncertainties to the simulated aerosols in the Arctic. High
468 resolution or regionally refined model is more desirable if resources allow. Given that
469 assumed injection heights of anthropogenic emissions in models are uncertain, the
470 ability to simulated surface aerosol concentrations and vertical distribution in models
471 could also be compromised (Yang et al., 2019b). In this study, we did not discuss the
472 effects of meteorological parameters on the long-term aerosol simulation mainly
473 because the decadal aerosol variation is dominated by changes in anthropogenic
474 emissions rather than meteorology (Yang et al., 2016).



475 ***Data availability.***

476 The CAM5 model is available at <http://www.cesm.ucar.edu/models/cesm1.2/> (last
477 access: 8 December 2019). Our CAM5-EAST model code and results can be made
478 available through the National Energy Research Scientific Computing Center (NERSC)
479 servers upon request.

480

481 ***Competing interests.***

482 The authors declare that they have no conflict of interest.

483

484 ***Author contribution.***

485 YY and HW designed the research; YY performed the model simulations; LR analyzed
486 the data. All the authors discussed the results and wrote the paper.

487

488 ***Acknowledgments.***

489 This research was support by the National Natural Science Foundation of China under
490 grant 41975159, Jiangsu Specially Appointed Professor Project and the U.S.
491 Department of Energy (DOE), Office of Science, Biological and Environmental
492 Research as part of the Earth and Environmental System Modeling program. The
493 Pacific Northwest National Laboratory is operated for DOE by Battelle Memorial
494 Institute under contract DE-AC05-76RLO1830. The National Energy Research
495 Scientific Computing Center (NERSC) provided computational support.

496



497 References

- 498 Alexeev, V. A., Esau, I., Polyakov, I. V., Byam, S. J., and Sorokina, S.: Vertical structure of recent
499 Arctic warming from observed data and reanalysis products, *Clim. Change*, 111, 215–239,
500 <https://doi.org/10.1007/s10584-011-0192-8>, 2012.
- 501 Bond, T. C., Doherty, S. J., Fahey, D. W., Forster, P. M., Berntsen, T., DeAngelo, B. J., Flanner, M.
502 G., Ghan, S., Kärcher, B., Koch, D., Kinne, S., Kondo, Y., Quinn, P. K., Sarofim, M. C., Schultz,
503 M. G., Schulz, M., Venkataraman, C., Zhang, H., Zhang, S., Bellouin, N., Guttikunda, S. K.,
504 Hopke, P. K., Jacobson, M. Z., Kaiser, J. W., Klimont, Z., Lohmann, U., Schwarz, J. P., Shindell,
505 D., Storelvmo, T., Warren, S. G., and Zender, C. S.: Bounding the role of black carbon in the
506 climate system: A scientific assessment, *J. Geophys. Res. Atmos.*, 118, 5380–5552,
507 <https://doi.org/10.1002/jgrd.50171>, 2013.
- 508 Boucher, O., Randall, D., Artaxo, P., Bretherton, C., Feingold, G., Forster, P., Kerminen, V.-M.,
509 Kondo, Y., Liao, H., Lohmann, U., Rasch, P., Satheesh, S. K., Sherwood, S., Stevens, B., and
510 Zhang, X. Y.: Clouds and Aerosols, in: *Climate Change 2013: The Physical Science Basis*,
511 Contribution of Working Group I to the Fifth Assessment Report of the Intergovernmental
512 Panel on Climate Change, edited by: Stocker, T. F., Qin, D., Plattner, G.-K., Tignor, M., Allen,
513 S. K., Boschung, J., Nauels, A., Xia, Y., Bex, V., and Midgley, P. M., Cambridge University
514 Press, Cambridge, UK and New York, NY, USA, 571–658,
515 <https://doi.org/10.1017/CBO9781107415324.016>, 2013.
- 516 Bourgeois, Q., and Bey, I.: Pollution transport efficiency toward the Arctic: Sensitivity to aerosol
517 scavenging and source regions, *J. Geophys. Res. Atmos.*, 116, D08213,
518 <https://doi.org/10.1029/2010JD015096>, 2011.
- 519 Breider, T. J., Mickley, L. J., Jacob, D. J., Wang, Q., Fisher, J. A., Chang, R. Y. W., and Alexander,
520 B.: Annual distributions and sources of Arctic aerosol components, aerosol optical depth, and
521 aerosol absorption, *J. Geophys. Res. Atmos.*, 119, 4107–4124,
522 <https://doi.org/10.1002/2013JD020996>, 2014.
- 523 Breider, T. J., Mickley, L. J., Jacob, D. J., Ge, C., Wang, J., Sulprizio Payer, M., Croft, B., Ridley, D.
524 A., McConnell, J. R., Sharma, S., Husain, L., Dutkiewicz, V. A., Eleftheriadis, K., Skov, H.,
525 and Hopke, P. K.: Multidecadal trends in aerosol radiative forcing over the Arctic: Contribution
526 of changes in anthropogenic aerosol to Arctic warming since 1980, *J. Geophys. Res. Atmos.*,
527 122, 3573–3594, <https://doi.org/10.1002/2016JD025321>, 2017.
- 528 Browse, J., Carslaw, K., Arnold, S., Pringle, K., and Boucher, O.: The scavenging processes
529 controlling the seasonal cycle in Arctic sulphate and black carbon aerosol, *Atmos. Chem. Phys.*,
530 12, 6775–6798, <https://doi.org/10.5194/acp-12-6775-2012>, 2012.
- 531 Dutkiewicz, V. A., DeJulio, A. M., Ahmed, T., Laing, J., Hopke, P. K., Skeie, R. B., Viisanen, Y.,
532 Paatero, J., and Husain, L.: Forty-seven years of weekly atmospheric black carbon
533 measurements in the Finnish Arctic: Decrease in black carbon with declining emissions, *J.*
534 *Geophys. Res. Atmos.*, 119, 7667–7683, <https://doi.org/10.1002/2014JD021790>, 2014.
- 535 Eckhardt, S., Quennehen, B., Olivié, D. J. L., Berntsen, T. K., Cherian, R., Christensen, J. H., Collins,
536 W., Crepinsek, S., Daskalakis, N., Flanner, M., Herber, A., Heyes, C., Hodnebrog, Ø., Huang,
537 L., Kanakidou, M., Klimont, Z., Langner, J., Law, K. S., Lund, M. T., Mahmood, R., Massling,
538 A., Myriokefalitakis, S., Nielsen, I. E., Nøjgaard, J. K., Quaas, J., Quinn, P. K., Raut, J.-C.,
539 Rumbold, S. T., Schulz, M., Sharma, S., Skeie, R. B., Skov, H., Uttal, T., von Salzen, K., and



- 540 Stohl, A.: Current model capabilities for simulating black carbon and sulfate concentrations in
541 the Arctic atmosphere: a multi-model evaluation using a comprehensive measurement data set,
542 *Atmos. Chem. Phys.*, 15, 9413–9433, <https://doi.org/10.5194/acp-15-9413-2015>, 2015.
- 543 Eleftheriadis, K., Vratolis, S., and Nyeki, S.: Aerosol black carbon in the European Arctic:
544 measurements at Zeppelin station, Ny-Ålesund, Svalbard from 1998–2007, *Geophys. Res.
545 Lett.*, 36, L02809, <https://doi.org/10.1029/2008GL035741>, 2009.
- 546 Fisher, J. A., Jacob, D. J., Wang, Q., Bahreini, R., Carouge, C. C., Cubison, M. J., Dibb, J. E., Diehl,
547 T., Jimenez, J. L., Leibensperger, E. M., Lu, Z., Meinders, M. B. J., Pye, H. O. T., Quinn, P. K.,
548 Sharma, S., Streets, D. G., van Donkelaar, A., and Yantosca, R. M.: Sources, distribution, and
549 acidity of sulfate–ammonium aerosol in the Arctic in winter–spring, *Atmos. Environ.*, 45,
550 7301–7318, <https://doi.org/10.1016/j.atmosenv.2011.08.030>, 2011.
- 551 Flanner, M. G., Zender, C. S., Randerson, J. T., and Rasch, P. J.: Present-day climate forcing and
552 response from black carbon in snow, *J. Geophys. Res.*, 112, D11202,
553 <https://doi.org/10.1029/2006JD008003>, 2007.
- 554 Flanner, M. G.: Arctic climate sensitivity to local black carbon, *J. Geophys. Res. Atmos.*, 118, 1840–
555 1851, <https://doi.org/10.1002/jgrd.50176>, 2013.
- 556 Garrett, T. J., Zhao, C., and Novelli, P.: Assessing the relative contributions of transport efficiency
557 and scavenging to seasonal variability in Arctic aerosol, *Tellus B*, 62, 190–196,
558 <https://doi.org/10.1111/j.1600-0889.2010.00453.x>, 2010.
- 559 Garrett, T. J., Brattström, S., Sharma, S., Worthy, D. E., and Novelli, P.: The role of scavenging in
560 the seasonal transport of black carbon and sulfate to the Arctic, *Geophys. Res. Lett.*, 38, L16805,
561 <https://doi.org/10.1029/2011GL048221>, 2011.
- 562 Gelaro, R., McCarty, W., Suárez, M. J., Todling, R., Molod, A., Takacs, L., Randles, C. A.,
563 Darmenov, A., Bosilovich, M. G., Reichle, R., Wargan, K., Coy, L., Cullather, R., Draper, C.,
564 Akella, S., Buchard, V., Conaty, A., da Silva, A. M., Gu, W., Kim, G.-K., Koster, R., Lucchesi,
565 R., Merkova, D., Nielsen, J. E., Partyka, G., Pawson, S., Putman, W., Rienecker, M., Schubert,
566 S. D., Sienkiewicz, M., and Zhao, B.: The Modern-Era Retrospective Analysis for Research
567 and 476 Applications, Version 2 (MERRA-2), *J. Climate*, 30, 5419–5454,
568 <https://doi.org/10.1175/JCLI-D-16-0758.1>, 2017.
- 569 Ghan, S. J., Liu, X., Easter, R. C., Zaveri, R., Rasch, P. J., Yoon, J. H., and Eaton, B.: Toward a
570 minimal representation of aerosols in climate models: Comparative decomposition of aerosol
571 direct, semidirect, and indirect radiative forcing, *J. Climate*, 25, 6461–6476,
572 <https://doi.org/10.1175/JCLI-D-11-00650.1>, 2012.
- 573 Gong, S. L., Zhao, T. L., Sharma, S., Toom-Sauntry, D., Lavoué, D., Zhang, X. B., Leaitch, W. R.,
574 and Barrie, L. A.: Identification of trends and interannual variability of sulfate and black carbon
575 in the Canadian High Arctic: 1981–2007, *J. Geophys. Res.*, 115, D07305,
576 <https://doi.org/10.1029/2009JD012943>, 2010.
- 577 Gravensén, R. G., Mauritsen, T., Tjernström, M., Källén, E., and Svensson, G.: Vertical structure of
578 recent Arctic warming, *Nature*, 451, 53–56, <https://doi.org/10.1038/nature06502>, 2008.
- 579 Heidam, N. Z., Wählin, P., and Christensen, J. H.: Tropospheric gases and aerosols in northeast
580 Greenland, *J. Atmos. Sci.*, 56, 261–278, [https://doi.org/10.1175/1520-0469\(1999\)056<0261:TGAAN>2.0.CO;2](https://doi.org/10.1175/1520-0469(1999)056<0261:TGAAN>2.0.CO;2), 1999.
- 582 Hirdman, D., Burkhardt, J. F., Sodemann, H., Eckhardt, S., Jefferson, A., Quinn, P. K., Sharma, S.,
583 Ström, J., and Stohl, A.: Long-term trends of black carbon and sulphate aerosol in the Arctic:



- 584 changes in atmospheric transport and source region emissions, *Atmos. Chem. Phys.*, 10, 9351-
585 9368, <https://doi.org/10.5194/acp-10-9351-2010>, 2010.
- 586 Hoesly, R. M., Smith, S. J., Feng, L., Klimont, Z., Janssens-Maenhout, G., Pitkanen, T., Seibert, J.
587 J., Vu, L., Andres, R. J., Bolt, R. M., Bond, T. C., Dawidowski, L., Kholod, N., Kurokawa, J.-
588 I., Li, M., Liu, L., Lu, Z., Moura, M. C. P., O'Rourke, P. R., and Zhang, Q.: Historical (1750–
589 2014) anthropogenic emissions of reactive gases and aerosols from the Community Emissions
590 Data System (CEDS), *Geosci. Model Dev.*, 11, 369–408, [https://doi.org/10.5194/gmd-11-369-](https://doi.org/10.5194/gmd-11-369-2018)
591 2018, 2018.
- 592 Koch, D., and Hansen, J.: Distant origins of Arctic black carbon: a Goddard Institute for Space
593 Studies ModelE experiment, *J. Geophys. Res.*, 110, D04204,
594 <https://doi.org/10.1029/2004JD005296>, 2005.
- 595 Koch, D., Schulz, M., Kinne, S., McNaughton, C., Spackman, J. R., Balkanski, Y., Bauer, S.,
596 Bernsten, T., Bond, T. C., Boucher, O., Chin, M., Clarke, A., De Luca, N., Dentener, F., Diehl,
597 T., Dubovik, O., Easter, R., Fahey, D. W., Feichter, J., Fillmore, D., Freitag, S., Ghan, S.,
598 Ginoux, P., Gong, S., Horowitz, L., Iversen, T., Kirkevåg, A., Klimont, Z., Kondo, Y., Krol, M.,
599 Liu, X., Miller, R., Montanaro, V., Moteki, N., Myhre, G., Penner, J. E., Perlwitz, J., Pitari, G.,
600 Reddy, S., Sahu, L., Sakamoto, H., Schuster, G., Schwarz, J. P., Seland, Ø., Stier, P., Takegawa,
601 N., Takemura, T., Textor, C., van Aardenne, J. A., and Zhao, Y.: Evaluation of black carbon
602 estimations in global aerosol models, *Atmos. Chem. Phys.*, 9, 9001–9026,
603 <https://doi.org/10.5194/acp-9-9001-2009>, 2009.
- 604 Law, K. S., and Stohl, A.: Arctic air pollution: Origins and impacts, *Science*, 315, 1537-1540,
605 <https://doi.org/10.1126/science>, 2007.
- 606 Lou, S., Yang, Y., Wang, H., Lu, J., Smith, S. J., Liu, F., and Rasch P. J.: Black carbon increases
607 frequency of extreme ENSO events, *J. Climate*, 32, 8323–8333, [https://doi.org/10.1175/JCLI-](https://doi.org/10.1175/JCLI-D-19-0549.1)
608 D-19-0549.1, 2019a.
- 609 Lou, S., Yang, Y., Wang, H., Smith, S. J., Qian, Y., and Rasch, P. J.: Black carbon amplifies haze
610 over the North China Plain by weakening the East Asian winter monsoon, *Geophys. Res. Lett.*,
611 46, 452–460, <https://doi.org/10.1029/2018GL080941>, 2019b.
- 612 McConnell, J. R., Edwards, R., Kok, G. L., Flanner, M. G., Zender, C. S., Saltzman, E. S., Banta, J.
613 R., Pasteris, D. R., Carter, M. M., and Kahl, J. D. W.: 20th-century industrial black carbon
614 emissions altered arctic climate forcing, *Science*, 317, 1381–1384,
615 <https://doi.org/10.1126/science.1144856>, 2007.
- 616 Mcfarquhar, G. M., and Wang, H.: Effects of aerosols on trade wind cumuli over the Indian Ocean:
617 Model simulations, *Q. J. R. Meteorol. Soc.*, 132, 821-843, <https://doi.org/10.1256/qj.04.179>,
618 2006.
- 619 Navarro, J. C. A., Varma, V., Riipinen, I., Seland, Ø., Kirkevåg, A., Struthers, H., Iversen, T.,
620 Hansson, H.-C., and Ekman, A. M. L.: Amplification of Arctic warming by past air pollution
621 reductions in Europe, *Nat. Geosci.*, 9, 277–281, <https://doi.org/10.1038/ngeo2673>, 2016.
- 622 O'Neill, N. T., Baibakov, K., Hesaraki, S., Ivanescu, L., Martin, R. V., Perro, C., Chaubey, J. P.,
623 Herber, A., and Duck, T. J.: Temporal and spectral cloud screening of polar winter aerosol
624 optical depth (AOD): impact of homogeneous and inhomogeneous clouds and crystal layers
625 on climatological-scale AODs, *Atmos. Chem. Phys.*, 16, 12753-12765,
626 <https://doi.org/10.5194/acp-16-12753-2016>, 2016.



- 627 Pithan, F. and Mauritsen, T.: Arctic amplification dominated by temperature feedbacks in
628 contemporary climate models, *Nat. Geosci.*, 7, 181–184, <https://doi.org/10.1038/ngeo2071>,
629 2014.
- 630 Polissar, A. V., Hopke, P. K., and Harris, J. M.: Source regions for atmospheric aerosol measured at
631 Barrow, Alaska, *Environ. Sci. Technol.*, 35, 4214–4226, <https://doi.org/10.1021/es0107529>,
632 2001.
- 633 Qi, L., Li, Q., Henze, D. K., Tseng, H.-L., and He, C.: Sources of springtime surface black carbon
634 in the Arctic: an adjoint analysis for April 2008, *Atmos. Chem. Phys.*, 17, 9697–9716,
635 <https://doi.org/10.5194/acp-17-9697-2017>, 2017.
- 636 Qian, Y., Yasunari, T. J., Doherty, S. J., Flanner, M. G., Lau, W. K., Ming, J., Wang, H., Wang, M.,
637 Warren, S. G., and Zhang, R.: Light-absorbing particles in snow and ice: Measurement and
638 modeling of climatic and hydrological impact, *Adv. Atmos. Sci.*, 32, 64–91,
639 <https://doi.org/10.1007/s00376-014-0010-0>, 2015.
- 640 Quaas, J., Ming, Y., Menon, S., Takemura, T., Wang, M., Penner, J. E., Gettelman, A., Lohmann, U.,
641 Bellouin, N., and Boucher, O.: Aerosol indirect effects—general circulation model
642 intercomparison and evaluation with satellite data, *Atmos. Chem. Phys.*, 9, 8697–8717,
643 <https://doi.org/10.5194/acp-9-8697-2009>, 2009.
- 644 Quinn, P., Shaw, G., Andrews, E., Dutton, E., Ruoho-Airola, T., and Gong, S.: Arctic haze: current
645 trends and knowledge gaps, *Tellus B*, 59, 99–114, <https://doi.org/10.1111/j.1600-0889.2006.00236.x>, 2007.
- 647 Quinn, P. K., Bates, T. S., Baum, E., Doubleday, N., Fiore, A. M., Flanner, M., Fridlind, A., Garrett,
648 T. J., Koch, D., Menon, S., Shindell, D., Stohl, A., and Warren, S. G.: Short-lived pollutants in
649 the Arctic: their climate impact and possible mitigation strategies, *Atmos. Chem. Phys.*, 8,
650 1723–1735, <https://doi.org/10.5194/acp-8-1723-2008>, 2008.
- 651 Quinn, P. K., Bates, T. S., Schulz, K., and Shaw, G. E.: Decadal trends in aerosol chemical
652 composition at Barrow, Alaska: 1976–2008, *Atmos. Chem. Phys.*, 9, 8883–8888,
653 <https://doi.org/10.5194/acp-9-8883-2009>, 2009.
- 654 Raatz, W. E., and Shaw, G. E.: Long-range tropospheric transport of pollution aerosols into the
655 Alaskan Arctic, *J. Clim. Appl. Meteor.*, 23, 1052–1064, <https://doi.org/10.1175/1520-0450>,
656 1984.
- 657 Rahn, K. A., Borys, R. D., and Shaw, G. E.: The Asian source of Arctic haze bands, *Nature*, 268,
658 713–715, <https://doi.org/10.1038/268713a0>, 1977.
- 659 Rahn, K. A.: Relative importances of North America and Eurasia as sources of Arctic aerosol, *Atmos.*
660 *Environ.*, 15, 1447–1455, [https://doi.org/10.1016/0004-6981\(81\)90351-6](https://doi.org/10.1016/0004-6981(81)90351-6), 1981.
- 661 Sand, M., Berntsen, T., Von Salzen, K., Flanner, M., Langner, J., and Victor, D.: Response of Arctic
662 temperature to changes in emissions of short-lived climate forcers, *Nat. Clim. Change*, 6, 286–
663 289, <https://doi.org/10.1038/nclimate2880>, 2016.
- 664 Screen, J. A., and Simmonds, I.: Increasing fall-winter energy loss from the Arctic Ocean and its
665 role in Arctic temperature amplification, *Geophys. Res. Lett.*, 37, L16707,
666 <https://doi.org/10.1029/2010GL044136>, 2010a.
- 667 Screen, J. A., and Simmonds, I.: The central role of diminishing sea ice in recent Arctic temperature
668 amplification, *Nature*, 464, 1334–1337, <https://doi.org/10.1038/nature09051>, 2010b.



- 669 Serreze, M. C., Barrett, A. P., Stroeve, J. C., Kindig, D. N., and Holland, M. M.: The emergence of
670 surface-based Arctic amplification, *The Cryosphere*, 3, 11–19, [https://doi.org/10.5194/tc-3-11-](https://doi.org/10.5194/tc-3-11-2009)
671 2009, 2009.
- 672 Sharma, S., Lavoué, D., Cachier, H., Barrie, L. A., and Gong, S. L.: Long-term trends of the black
673 carbon concentrations in the Canadian Arctic, *J. Geophys. Res. Atmos.*, 109, D15203,
674 <https://doi.org/10.1029/2003JD004331>, 2004.
- 675 Sharma, S., Andrews, E., Barrie, L., Ogren, J., and Lavoué, D.: Variations and sources of the
676 equivalent black carbon in the high Arctic revealed by long-term observations at Alert and
677 Barrow: 1989–2003, *J. Geophys. Res.*, 111, D14208, <https://doi.org/10.1029/2005JD006581>,
678 2006.
- 679 Sharma, S., Ishizawa, M., Chan, D., Lavoué, D., Andrews, E., Eleftheriadis, K., and Maksyutov, S.:
680 16-year simulation of Arctic black carbon: Transport, source contribution, and sensitivity
681 analysis on deposition, *J. Geophys. Res. Atmos.*, 118, 943–964,
682 <https://doi.org/10.1029/2012JD017774>, 2013.
- 683 Sharma, S., Leaitch, W. R., Huang, L., Veber, D., Kolonjari, F., Zhang, W., Hanna, S. J., Bertram,
684 A. K., and Ogren, J. A.: An Evaluation of three methods for measuring black carbon at Alert,
685 Canada, *Atmos. Chem. Phys.*, 17, 15225–15243, <https://doi.org/10.5194/acp-2017-339>, 2017.
- 686 Shindell, D. T., Chin, M., Dentener, F., Doherty, R. M., Faluvegi, G., Fiore, A. M., Hess, P., Koch,
687 D. M., MacKenzie, I. A., Sanderson, M. G., Schultz, M. G., Schulz, M., Stevenson, D. S., Teich,
688 H., Textor, C., Wild, O., Bergmann, D. J., Bey, I., Bian, H., Cuvelier, C., Duncan, B. N.,
689 Folberth, G., Horowitz, L. W., Jonson, J., Kaminski, J. W., Marmor, E., Park, R., Pringle, K. J.,
690 Schroeder, S., Szopa, S., Takemura, T., Zeng, G., Keating, T. J., and Zuber, A.: A multi-model
691 assessment of pollution transport to the Arctic, *Atmos. Chem. Phys.*, 8, 5353–5372,
692 <https://doi.org/10.5194/acp-8-5353-2008>, 2008.
- 693 Shindell, D., and Faluvegi, G.: Climate response to regional radiative forcing during the twentieth
694 century, *Nat. Geosci.*, 2, 294–300, <https://doi.org/10.1038/ngeo473>, 2009.
- 695 Sinha, P. R., Kondo, Y., Koike, M., Ogren, J. A., Jefferson, A., Barrett, T. E., Sheesley, R. J., Ohata,
696 S., Moteki, N., Coe, H., Liu, D., Irwin, M., Tunved, P., Quinn, P. K. and Zhao, Y.: Evaluation
697 of ground-based black carbon measurements by filter-based photometers at two Arctic sites, *J.*
698 *Geophys. Res. Atmos.*, 122, 3544–3572, <https://doi.org/10.1002/2016JD025843>, 2017.
- 699 Sirois, A., and Barrie, L. A.: Arctic lower tropospheric aerosol trends and composition at Alert,
700 Canada: 1980–1995, *J. Geophys. Res. Atmos.*, 104, 11599–11618,
701 <https://doi.org/10.1029/1999JD900077>, 1999.
- 702 Stohl, A.: Characteristics of atmospheric transport into the Arctic troposphere, *J. Geophys. Res.*, 111,
703 D11306, <https://doi.org/10.1029/2005JD006888>, 2006.
- 704 Trenberth, K., Jones, P., Ambenje, P., Bojariu, R., Easterling, D., Klein Tank, A., Parker, D.,
705 Rahimzadeh, F., Renwick, J., and Rusticucci, M.: Observations: surface and atmospheric
706 climate change. chap. 3 of *Climate Change: The Physical Science Basis*, in *Contribution of*
707 *Working Group I to the Fourth Assessment Report of the Intergovernmental Panel on Climate*
708 *Change*, edited by S. Solomon et al., 235–336, Cambridge Univ. Press, Cambridge, U. K., and
709 New York, 2007.
- 710 Twomey, S.: Pollution and the planetary albedo, *Atmos. Environ.*, 8, 1251–1256,
711 [https://doi.org/10.1016/0004-6981\(74\)90004-3](https://doi.org/10.1016/0004-6981(74)90004-3), 1974.



- 712 Wang, H., Easter, R. C., Rasch, P. J., Wang, M., Liu, X., Ghan, S. J., Qian, Y., Yoon, J.-H., Ma, P.-
713 L., and Vиноj, V.: Sensitivity of remote aerosol distributions to representation of cloud–aerosol
714 interactions in a global climate model, *Geosci. Model Dev.*, 6, 765–782,
715 <https://doi.org/10.5194/gmd-6-765-2013>, 2013.
- 716 Wang, H., Rasch, P. J., Easter, R. C., Singh, B., Zhang, R., Ma, P. L., Qian, Y., Ghan, S. J., and
717 Beagley, N.: Using an explicit emission tagging method in global modeling of source-receptor
718 relationships for black carbon in the Arctic: Variations, sources, and transport pathways, *J.*
719 *Geophys. Res.*, 119, 12,888–12,909, <https://doi.org/10.1002/2014JD022297>, 2014.
- 720 Yang, Y., Liao, H., and Lou, S.: Increase in winter haze over eastern China in recent decades: Roles
721 of variations in meteorological parameters and anthropogenic emissions, *J. Geophys. Res.*, 121,
722 13, 050–13, 065, <https://doi.org/10.1002/2016JD025136>, 2016.
- 723 Yang, Y., Wang, H., Smith, S. J., Easter, R., Ma, P.-L., Qian, Y., Yu, H., Li, C., and Rasch, P. J.:
724 Global source attribution of sulfate concentration and direct and indirect radiative forcing,
725 *Atmos. Chem. Phys.*, 17, 8903–8922, <https://doi.org/10.5194/acp-17-8903-2017>, 2017a.
- 726 Yang, Y., Wang, H., Smith, S. J., Ma, P.-L., and Rasch, P. J.: Source attribution of black carbon and
727 its direct radiative forcing in China, *Atmos. Chem. Phys.*, 17, 4319–4336,
728 <https://doi.org/10.5194/acp-17-4319-2017>, 2017b.
- 729 Yang, Y., Wang, H., Smith, S. J., Easter, R. C., and Rasch, P. J.: Sulfate aerosol in the Arctic: Source
730 attribution and radiative forcing, *J. Geophys. Res.*, 123, 1899–1918,
731 <https://doi.org/10.1002/2017JD027298>, 2018a.
- 732 Yang, Y., Wang, H., Smith, S. J., Zhang, R., Lou, S., Qian, Y., Ma, P.-L., and Rasch, P. J.: Recent
733 intensification of winter haze in China linked to foreign emissions and meteorology, *Sci. Rep.*,
734 8, 2107, <https://doi.org/10.1038/s41598-018-20437-7>, 2018b.
- 735 Yang, Y., Wang, H., Smith, S. J., Zhang, R., Lou, S., Yu, H., Li, C., and Rasch, P. J.: Source
736 apportionments of aerosols and their direct radiative forcing and long-term trends over
737 continental United States, *Earth's Future*, 6, 793–808, <https://doi.org/10.1029/2018EF000859>,
738 2018c.
- 739 Yang, Y., Smith, S. J., Wang, H., Lou, S., and Rasch, P. J.: Impact of anthropogenic emission
740 injection height uncertainty on global sulfur dioxide and aerosol distribution, *J. Geophys.*
741 *Res.*, 124, 4812–4826, <https://doi.org/10.1029/2018JD030001>, 2019a.
- 742 Yang, Y., Smith, S. J., Wang, H., Mills, C. M., and Rasch, P. J.: Variability, timescales, and
743 nonlinearity in climate responses to black carbon emissions, *Atmos. Chem. Phys.*, 19, 2405–
744 2420, <https://doi.org/10.5194/acp-19-2405-2019>, 2019b.
- 745 Zamora, L. M., Kahn, R. A., Eckhardt, S., McComiskey, A., Sawamura, P., Moore, R., and Stohl,
746 A.: Aerosol indirect effects on the nighttime Arctic Ocean surface from thin, predominantly
747 liquid clouds, *Atmos. Chem. Phys.*, 17, 7311–7332, <https://doi.org/10.5194/acp-17-7311-2017>,
748 2017.
- 749 Zhang, R., Wang, H., Fu, Q., Pendergrass, A. G., Wang, M., Yang, Y., Ma P.-L., and Rasch, P. J.:
750 Local radiative feedbacks over the Arctic based on observed short-term climate variations,
751 *Geophys. Res. Lett.*, 45, 5761–5770, <https://doi.org/10.1029/2018GL077852>, 2018.
- 752 Zhang, R., Wang, H., Fu, Q., Rasch, P. J., and Wang, X.: Unraveling driving forces explaining
753 significant reduction in satellite-inferred Arctic surface albedo since the 1980s, *P. Natl. Acad.*
754 *Sci. USA*, 116, 23947–23953, <https://doi.org/10.1073/pnas.1915258116>, 2019.



755 Zhao, C., and Garrett, T. J.: Effects of Arctic haze on surface cloud radiative forcing, *Geophys. Res.*
756 *Lett.*, 42, 557-564, <https://doi.org/10.1002/2014GL062015>, 2015.

757



758 **Table 1.** Contributions of emissions from major source regions to the simulated
759 annual mean near-surface sulfate and BC concentrations ($\mu\text{g m}^{-3}$) averaged over the
760 Arctic in 1980–1984 and 2014–2018, as well as the percentage differences (%)
761 between 1980–1984 and 2014–2018 relative to 1980–1984.
762

	Sulfate Conc.		
	1980-1984	2014-2018	Last 5 -First 5
Sum	0.447	0.256	-42.83%
ARC	0.15	0.141	-2.02%
EUR	0.097	0.014	-18.61%
NAM	0.022	0.007	-3.36%
CAS	0.013	0.006	-1.57%
RBU	0.129	0.045	-18.83%
OCN	0.029	0.032	0.67%
OTH	0.006	0.01	0.90%

	BC Conc.		
	1980-1984	2014-2018	Last 5 -First 5
Sum	0.0161	0.0124	-22.98%
ARC	0.0086	0.0071	-9.32%
EUR	0.0011	0.0006	-3.11%
NAM	0.0004	0.0009	3.11%
EAS	0.0002	0.0003	0.62%
RBU	0.0056	0.0032	-14.91%
OTH	0.0002	0.0003	0.62%

763



764 **Table 2.** Trends in annual mean sulfate and BC concentrations (% per decade) in
765 surface air and in the column contributed by 16 anthropogenic source regions during
766 1980–2018 relative to the 39-year averages.
767

Region	Sulfate Conc.	Sulfate Burden	BC Conc.	BC Burden
Sum	-19.83%	-13.18%	-11.93%	3.98%
EUR	-8.42%	-10.30%	-1.61%	-2.26%
NAM	-1.52%	-3.90%	0.96%	1.45%
CAM	0.00%	0.05%	0.00%	-0.01%
SAM	0.00%	-0.03%	0.00%	0.01%
NAF	0.02%	0.12%	0.05%	0.51%
SAF	0.00%	-0.02%	0.00%	0.18%
MDE	0.09%	0.85%	0.04%	0.79%
SEA	0.00%	0.11%	0.00%	0.09%
CAS	-0.72%	-1.01%	-0.04%	-0.05%
SAS	0.06%	3.49%	0.04%	1.97%
EAS	0.45%	4.24%	0.43%	5.90%
RBU	-8.54%	-6.64%	-6.12%	-3.74%
PAN	0.00%	0.00%	0.00%	0.00%
ARC	-1.38%	-0.20%	-5.96%	-1.01%
ANT	0.00%	0.00%	0.00%	0.00%
OCN	0.14%	0.08%	0.27%	0.16%

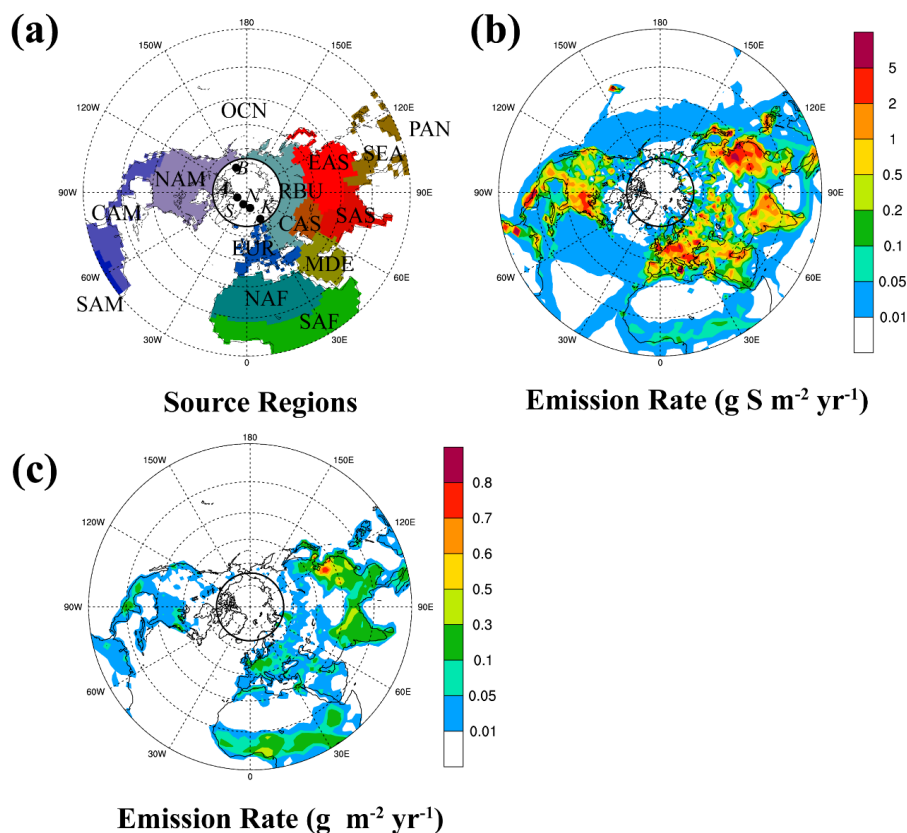
768



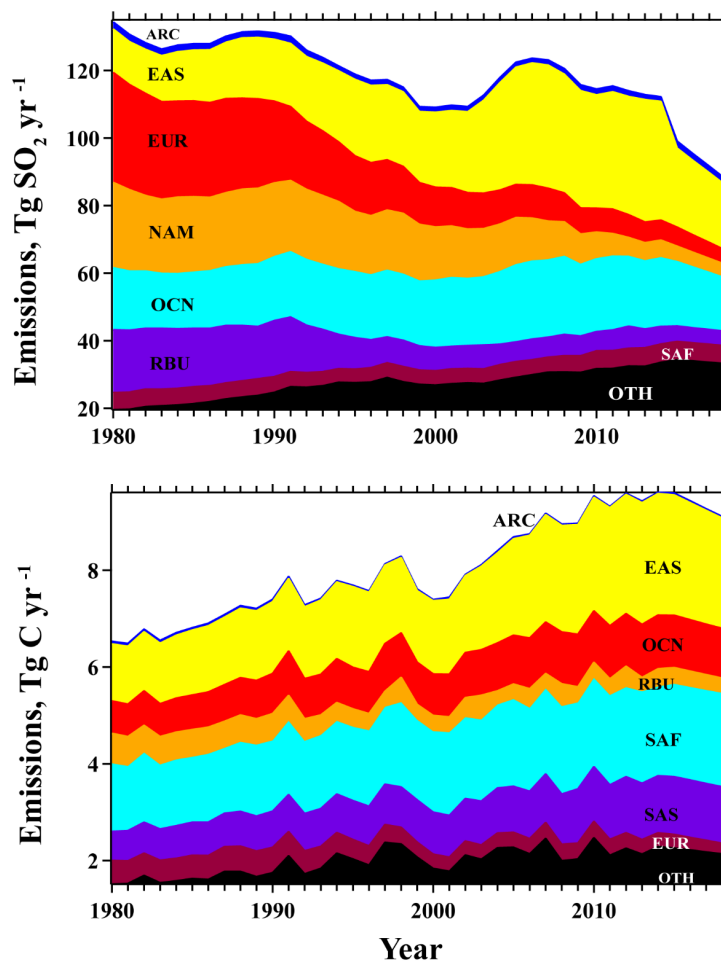
769 **Table 3.** Estimated annual mean of the response in Arctic surface temperatures (K) to
770 the change in TOA radiative forcing due to aerosol-radiation interactions (RF_{ari}) of
771 sulfate and BC, aerosol-cloud interactions (RF_{aci}) of sulfate and radiative forcing (RF)
772 due to BC in snow/ice ($W\ m^{-2}$) in each latitude band. The Arctic equilibrium
773 temperature response is estimated using Arctic climate sensitivity factors (λ , $K\ W^{-1}$
774 m^2), defined as the change in Arctic surface temperature per unit RF, for different
775 latitudinal bands from Sand et al. (2016) and Shindell and Faluvegi (2009).
776

Forcing location	Arctic equilibrium surface temperature response (K)*			
	Sulfate RF_{ari}	Sulfate RF_{aci}	BC RF_{ari}	BC snow/ice
60°N - 90°N	0.035	0.078	-0.005	-0.061
28°N - 60°N	0.059	0.165	0.029	0.019
28°S - 28°N	-0.001	-0.048	0.031	0.000
90°S - 28°S	-0.005	-0.002	0.002	0.000
SUM	0.088	0.193	0.057	-0.041

777 *The λ are 0.31, 0.17, 0.16, 0.06 for sulfate RF_{ari} and RF_{aci} ; -0.08, 0.15, 0.31, 0.06 for
778 BC RF_{ari} ; 1.06, 0.45, 0.93, 0.18 for RF due to BC in snow/ice, according to the order
779 given by forcing locations in the table. Sulfate RF_{aci} is not archived in this study and is
780 roughly estimated here by scaling sulfate RF_{ari} based on the ratio of sulfate RF_{aci} and
781 RF_{ari} over different latitudes from Sand et al. (2016).

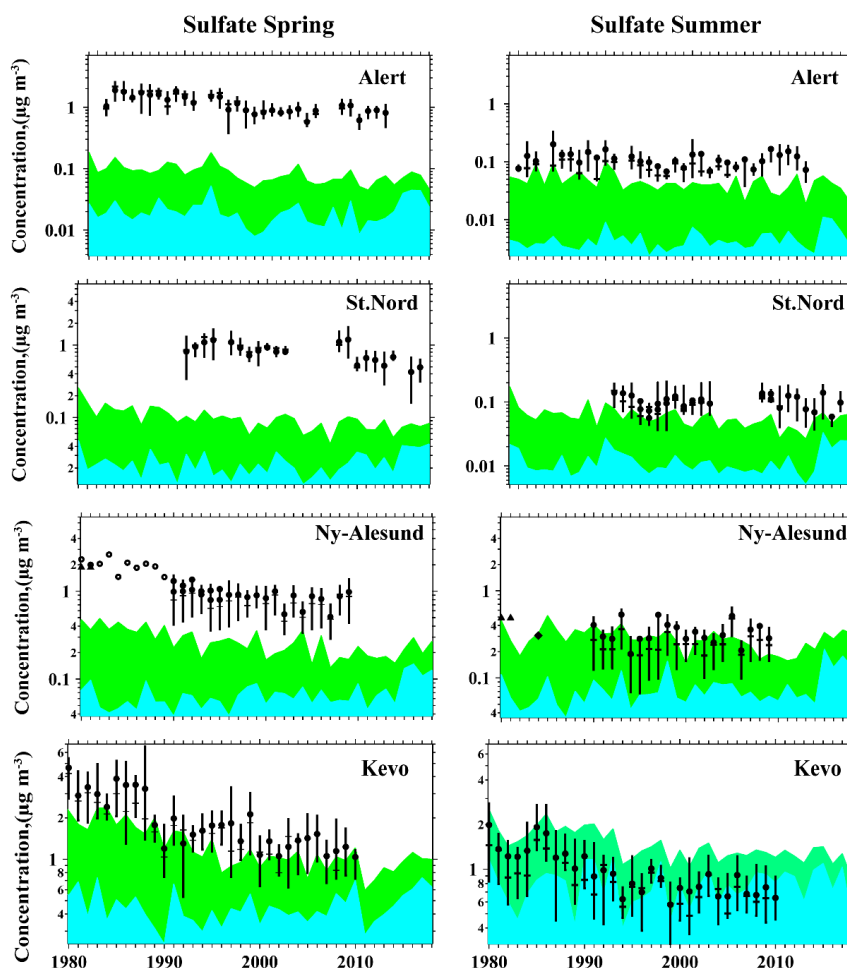


782
783 **Figure 1.** (a) Sixteen anthropogenic source regions (Europe (EUR), North America
784 (NAM), Central America (CAM), South America (SAM), North Africa (NAF), South
785 Africa (SAF), the Middle East (MDE), Southeast Asia (SEA), Central Asia (CAS),
786 South Asia (SAS), East Asia (EAS), Russia-Belarus-Ukraine (RBU), Pacific-Australia-
787 New Zealand (PAN), the Arctic (ARC), Antarctic (ANT), and Non-Arctic/Antarctic
788 Ocean (OCN)). Spatial distribution of annual mean (b) SO_2 ($\text{g S m}^{-2} \text{yr}^{-1}$) and (c) BC (g
789 $\text{C m}^{-2} \text{yr}^{-1}$) emissions averaged over 1980-2018. The thick black circle represents the
790 Arctic (66.5°N – 90°N). Dots in (a) are observational sites at Alert (“A”, 82°N , 62°W),
791 Station Nord (“S”, 81°N , 16°W), Barrow (“B”, 71°N , 156°W), Ny-Alesund (“N”, 78°N ,
792 11°E) and Kevo (“K”, 69°N , 27°E).

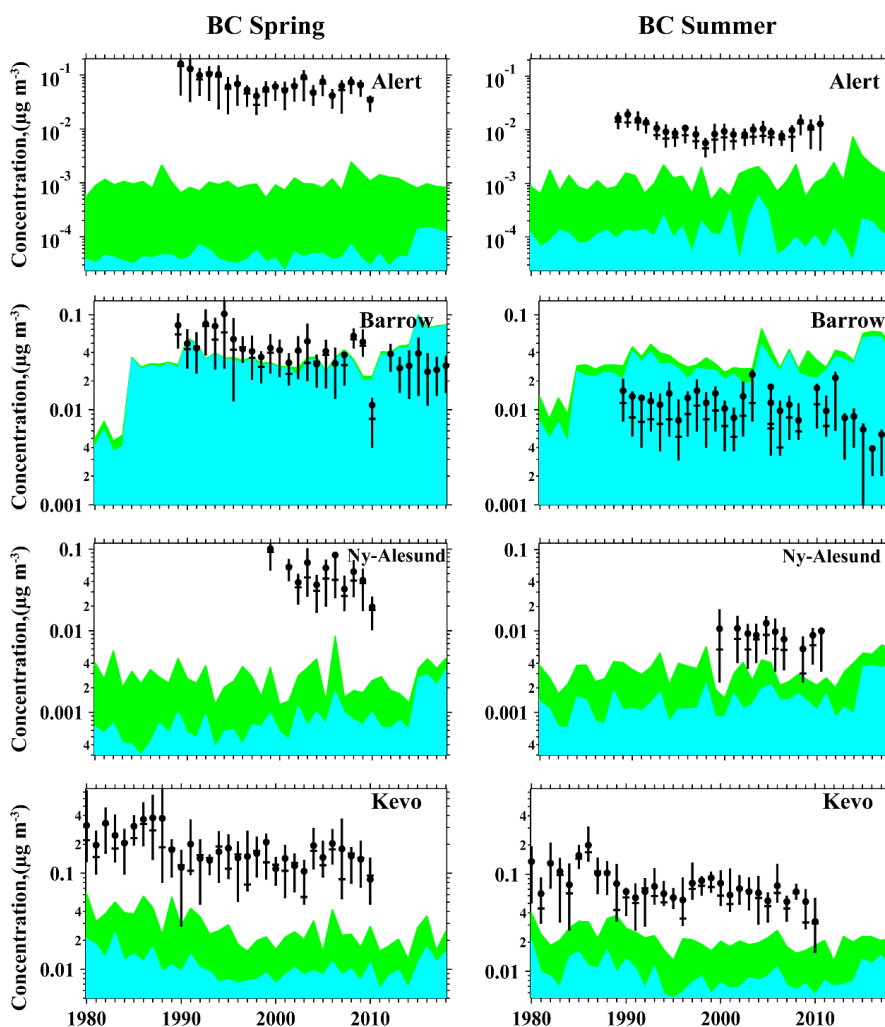


793

794 **Figure 2.** Time series of global total anthropogenic emissions of (top) SO₂ (Tg SO₂ yr⁻¹) and (bottom) BC (Tg C yr⁻¹), classified by key anthropogenic source regions.
795

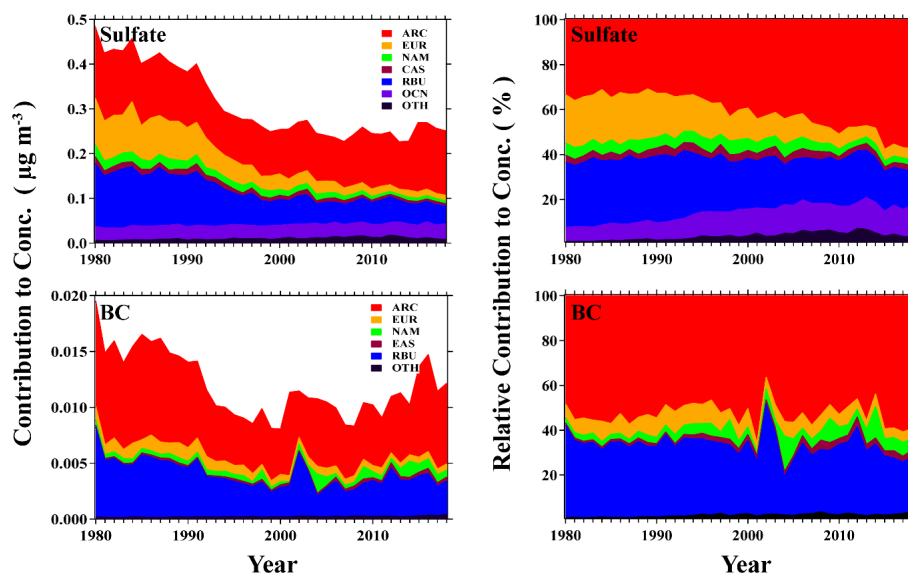


796
797 **Figure 3.** Surface concentrations of sulfate aerosols ($\mu\text{g m}^{-3}$) in spring (March–May)
798 and summer (June–August) at four locations (Alert, Station Nord, Ny-Alesund, Kevo)
799 in the Arctic during 1980–2018. Seasonal means are denoted by solid black circles,
800 medians as short horizontal bars, and the 25th to 75th percentile ranges as vertical bars.
801 Stacked contours represent the Arctic (blue) and non-Arctic anthropogenic source
802 region (green) contributions to the modeled concentrations.

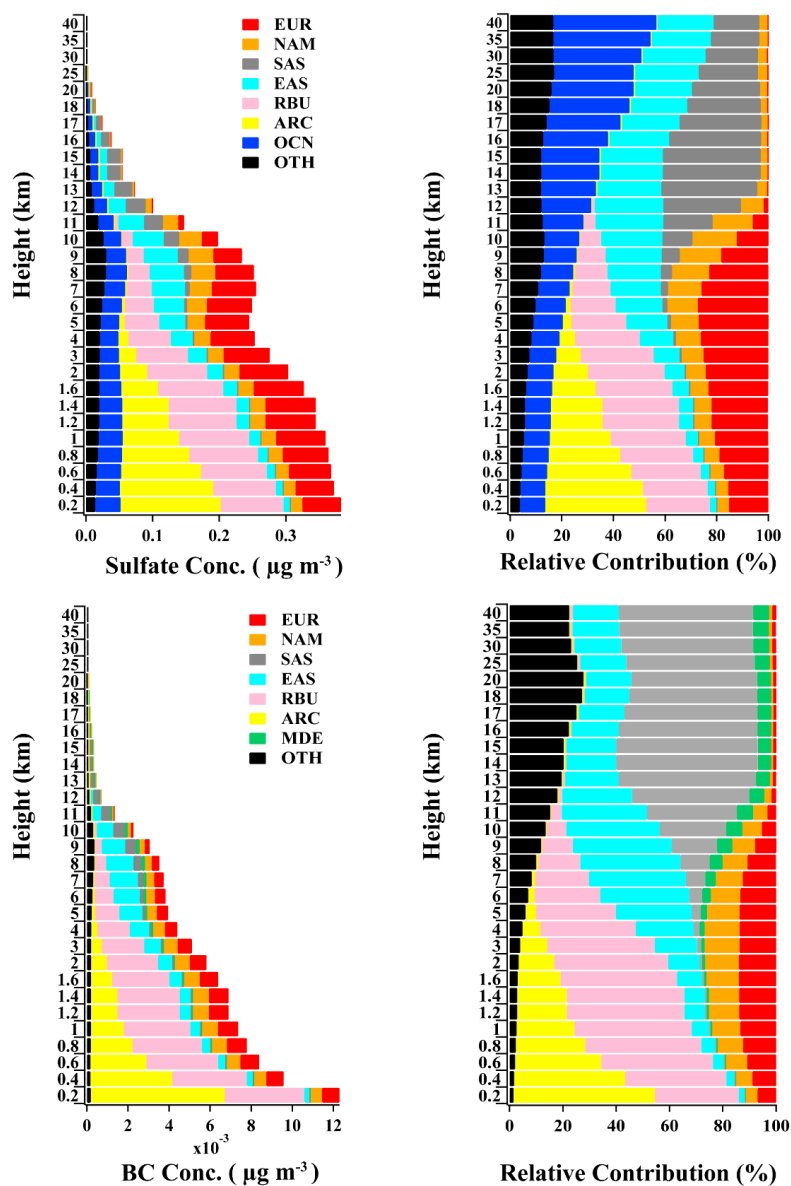


803

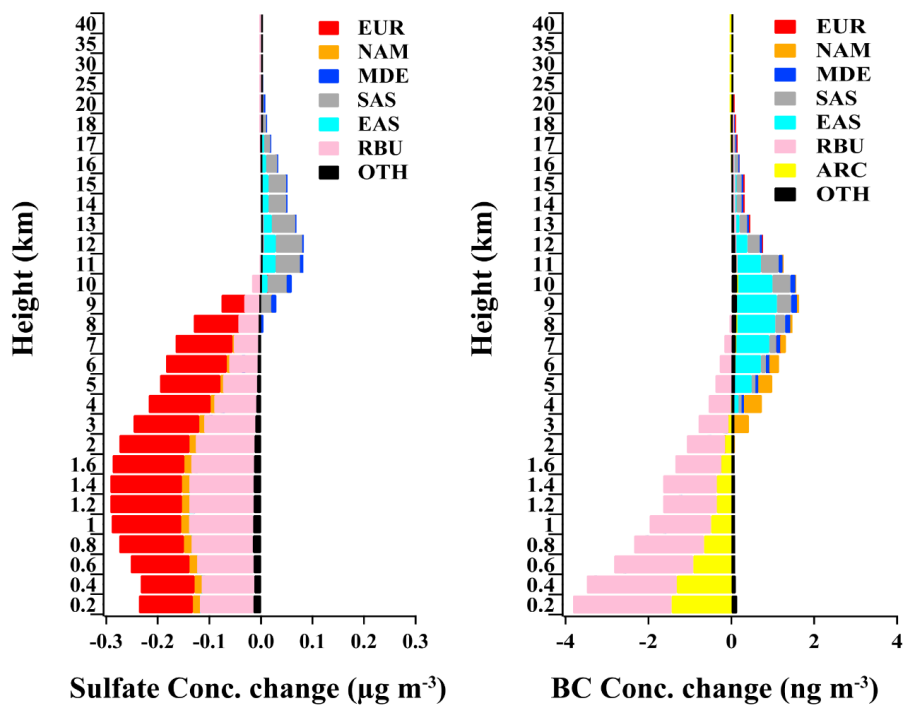
804 **Figure 4.** Same as Figure 3, but for surface BC ($\mu\text{g m}^{-3}$) at four (Alert, Barrow, Ny-
805 Alesund, Kevo) Arctic sites.



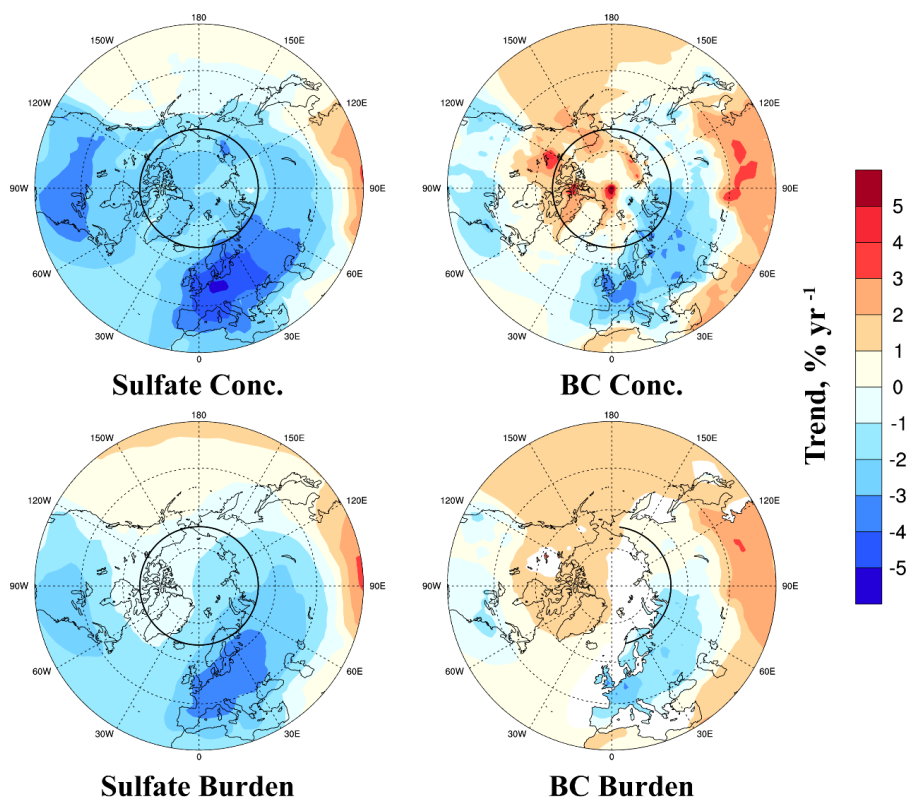
806
807 **Figure 5.** Time series (1980–2018) of absolute (left, $\mu\text{g m}^{-3}$) and relative (right, %) contributions of emissions from major source regions to the simulated annual mean
808 near-surface sulfate and BC concentrations averaged over the Arctic.
809



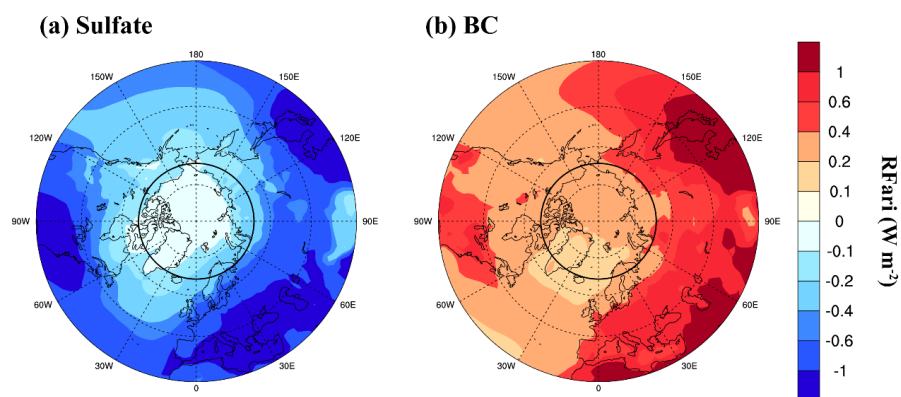
810
 811 **Figure 6.** Annual mean vertical profile of sulfate (top) and BC (bottom) concentrations
 812 ($\mu\text{g m}^{-3}$) over the Arctic contributed by the tagged source regions (left) and their relative
 813 contributions (right, %) during 1980–2018. Sources with annual burden contributions
 814 less than 5% are combined and shown as OTH.



815
816 **Figure 7.** Changes in annual mean vertical profile of sulfate ($\mu\text{g m}^{-3}$, left) and BC (ng m^{-3} , right) concentrations over the Arctic contributed by the tagged source regions
817 m^{-3} , right) concentrations over the Arctic contributed by the tagged source regions
818 between 1980–1984 and 2014–2018.

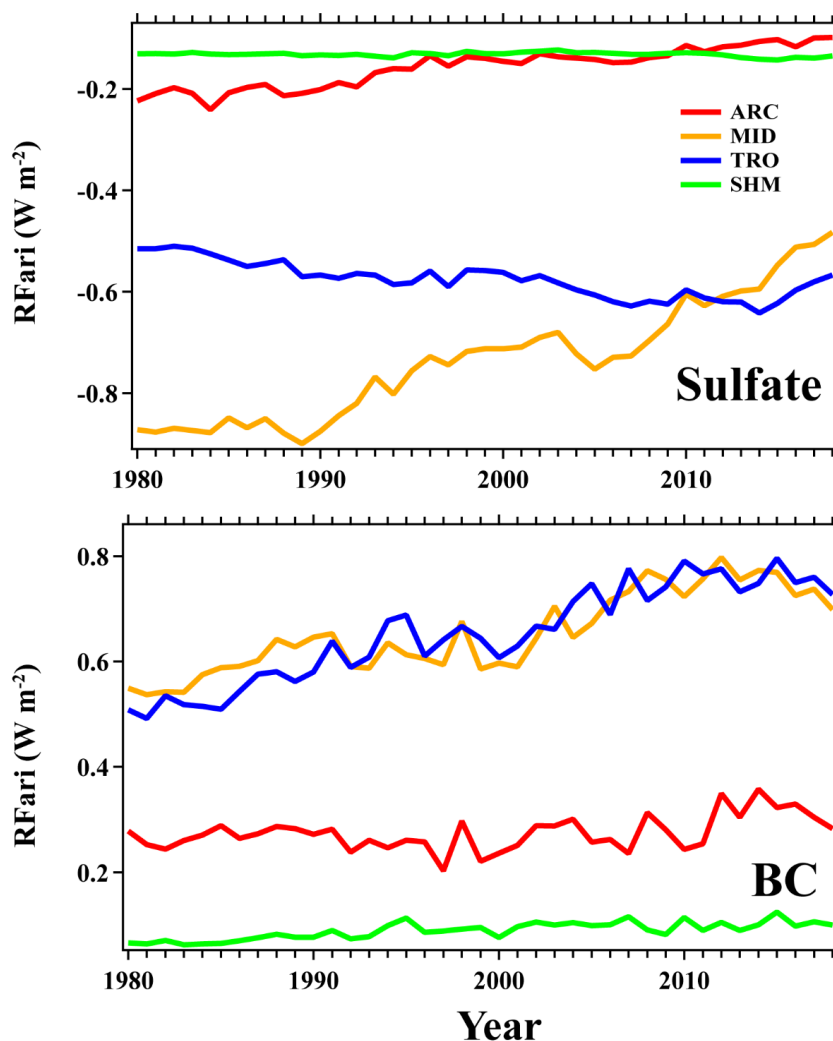


819
820 **Figure 8.** Spatial distribution of linear trends in annual mean sulfate (left) and BC (right)
821 concentrations (% yr⁻¹) near the surface (top) and column burden (bottom) relative to
822 the 39-year averages.

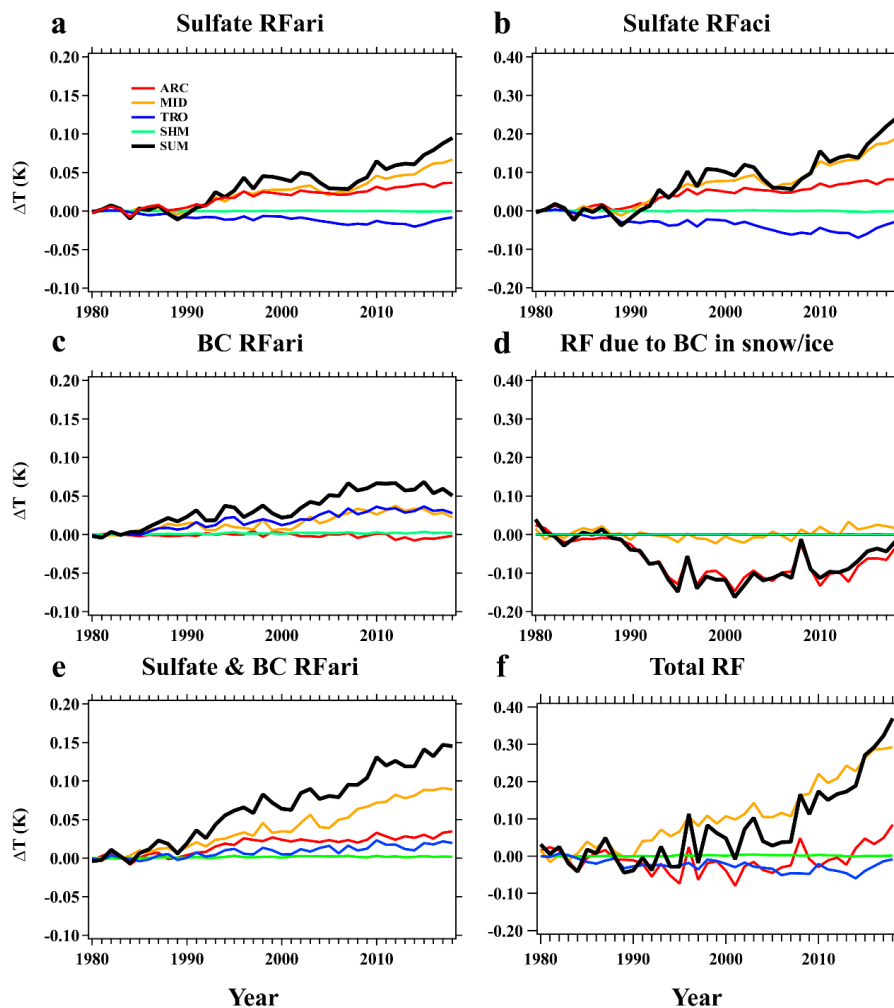


823

824 **Figure 9.** Spatial distribution of annual mean radiative forcing due to aerosol-radiation
825 interactions (RF_{ari}) of (a) sulfate and (b) BC ($W m^{-2}$) at the TOA averaged over 1980–
826 2018.



827
828 **Figure 10.** Time series (1980–2018) of annual radiative forcing due to aerosol-radiation
829 interactions (RF_{ari} , W m^{-2}) of sulfate and BC over the Arctic (ARC, 66.5°N – 90°N),
830 Northern Hemisphere mid-latitudes (MID, 28°N – 66.5°N), tropics (TRO, 28°S – 28°N)
831 and Southern Hemisphere (SHM, 90°S – 28°S).



832

833 **Figure 11.** Time series (1980–2018) of the estimated response in surface temperatures
834 (K) to the change in radiative forcing due to the aerosol-radiation interactions (RF_{ari}) of
835 (a) sulfate, (c) BC, and (e) sum of sulfate and BC RF_{ari} , (b) radiative forcing due to
836 aerosol-cloud interactions (RF_{aci}) of sulfate, (d) radiative forcing (RF) due to BC in
837 snow/ice, (f) sum of all RF in each latitude bands and the sum of them (SUM).